

# Fault Detection, Real-Time Error Recovery, and Experimental Demonstration for Digital Microfluidic Biochips\*

Kai Hu, Bang-Ning Hsu, Andrew Madison, Krishnendu Chakrabarty and Richard Fair

**Abstract**—Advances in digital microfluidics and integrated sensing hold promise for a new generation of droplet-based biochips that can perform multiplexed assays to determine the identity of target molecules. Despite these benefits, defects and erroneous fluidic operations remain a major barrier to the adoption and deployment of these devices. We describe the first integrated demonstration of cyberphysical coupling in digital microfluidics, whereby errors in droplet transportation on the digital microfluidic platform are detected using capacitive sensors, the test outcome is interpreted by control hardware, and software-based error recovery is accomplished using dynamic reconfiguration. The hardware/software interface is realized through seamless interaction between control software, an off-the-shelf microcontroller and a frequency divider implemented on an FPGA. Experimental results are reported for a fabricated silicon device and links to videos are provided for the first-ever experimental demonstration of cyberphysical coupling and dynamic error recovery in digital microfluidic biochips.

## I. INTRODUCTION

Digital (droplet-based) microfluidics is an emerging technology that enables the integration of fluid-handling operations on a biochip [1]. Liquid droplets with picoliter volumes in a digital microfluidic biochip can be manipulated on an array of discrete unit cells [2]. Fluid-handling operations, such as dilution of samples and reagents, mixing, incubation and transportation of droplets, can be implemented on the biochip by applying appropriate voltages to the electrodes [3]. The sequence of actuation voltages is pre-determined (i.e., before the implementation of fluid-handling operations), and they are stored in a microcontroller or in computer memory. Under clock control, the microcontroller transfers preloaded actuation data to the biochip.

Advances in microfluidics and integrated sensing hold promise for a newer generation of biochips, which can perform biochemical reactions in real-time and autonomously for applications such as point-of-care clinical diagnostics. Since droplets in digital microfluidics can be actuated using voltages, the entire integrated microfluidics and sensing system can be controlled using software. The software can use sensed information to reconfigure the system for error recovery and for further processing of samples based upon real-time sensing of droplets. This level of integration, decision, and controlled

reconfigurability is a significant step forward in diagnostic platforms.

Despite the above potential benefits, defects and erroneous fluidic operations remain a major barrier to adoption and deployment. Moreover, due to the inherent randomness and complexity of the component interactions that are ubiquitous in biochemistry, predictive modeling and accuracy control are difficult [4], [5]. Yet, despite such inherent variability, many biomedical experiments, such as drug development and clinical diagnostics, require fluid-handling operations that are highly accurate and precise. If an unexpected error occurs during the experiment, the outcome of the entire experiment will be incorrect. When this occurs, all the steps of the experiment must be repeated to correct the error [6]. Repetition of experiments leads to wastage of time, expensive reagents and hard-to-obtain samples.

To avoid repetitive execution of on-chip biochemical experiments, a cyberphysical system implementation of a biochip has recently been proposed [7], [8]. The key idea here is that control software is used to reconfigure the biochip based on real-time feedback from on-chip sensors. The system design in [7], [8] was however only conceptual in nature and important details such as error detection, hardware/software interface, and programmable software-based control were not addressed. The work in [7] also requires human intervention through control software running on a computer, which increases the complexity of the cyberphysical system.

In this paper, we present a physical set-up for testing, error detection, and demonstration of the coordination between hardware (biochip and sensors) and control software. We describe the first integrated demonstration of cyberphysical coupling in digital microfluidics, whereby errors in droplet transportation on the digital microfluidic platform are detected using capacitive sensors, the test outcome is interpreted by control hardware, and software-based recovery is accomplished using dynamic reconfiguration. The hardware/software interface is realized through seamless interaction between control software, an off-the-shelf microcontroller, a shift register for electrode addressing, and a frequency divider implemented on an FPGA. Experimental results are reported for a fabricated silicon device and links to videos [13] are provided for the first-ever experimental demonstration of cyberphysical coupling and dynamic error recovery in digital microfluidic biochips. The demonstration highlights real-time control of multiple droplets, autonomous error detection through capacitance sensing, and re-routing of droplets to bypass fault sites

\*The work was supported by the US National Science Foundation under grants CCF-0914895 and CNS-1135853.

without any human intervention.

The rest of paper is organized as follows. Section II describes fabrication defects and fault models for digital microfluidic biochips, capacitance sensing and cyberphysical error recovery. While fabrication defects for digital microfluidics have been characterized [9], [10] and capacitance sensing presented in prior work [11], [12], this is the first time to attempt to evaluate such an error detection method for a fabricated biochip. The basic capacitance sensing approach was found to be insufficient for error detection. Hence additional circuitry was added to the sensor design. The demonstration of cyberphysical error recovery experimental setup are discussed in Section III. The proposed error recovery procedure is based on the notion of a region-based division of the biochip. We present the layout of fabricated biochip and describe the hardware/software interface and the control system. Microfluidic biochip fabrication, capacitance sensor realization, and results and videos are discussed in Section IV. Section V concludes the paper.

## II. DEFECTS, TESTING, AND RECOVERY SOLUTION

In this section, we describe typical defects in fabricated biochips, fault detection using capacitance sensing, and error recovery based on the hardware/software interface.

### A. Defects and Fault Models

A digital microfluidic biochip is said to have a failure if its operation does not match its specified behavior [1]. In order to detect defects using electrical methods, fault models that efficiently represent the effect of physical defects at some level of abstraction are required. These models can be used to capture the effect of physical defects that produce incorrect behavior. Faults can be caused by manufacturing imperfections, or by degradation during use as we apply alternating high and low voltages to electrodes. Some typical defects are listed below.

- *Dielectric breakdown*: The breakdown of the dielectric at high voltage levels creates a short between the droplet and the electrode. When this happens, the droplet undergoes electrolysis, which prevents transportation.
- *Short between the adjacent electrodes*: If a short occurs between two adjacent electrodes, the two electrodes effectively form one longer electrode. When a droplet resides on this electrode, it is no longer large enough to overlap the gap between adjacent electrodes. As a result, the actuation of the droplet can no longer be achieved.
- *Degradation of the insulator*: This degradation effect is unpredictable and may become apparent gradually during operation. Degradation is often caused due to irreversible charge concentration near the electrodes due to actuation over long durations. A consequence is that droplets often fragment and their motion is prevented because of the unwanted variation of surface tension forces along their flow path.
- *Open in the metal connection between the electrode and the control source*: This defect results in a failure in activating the electrode for transport.

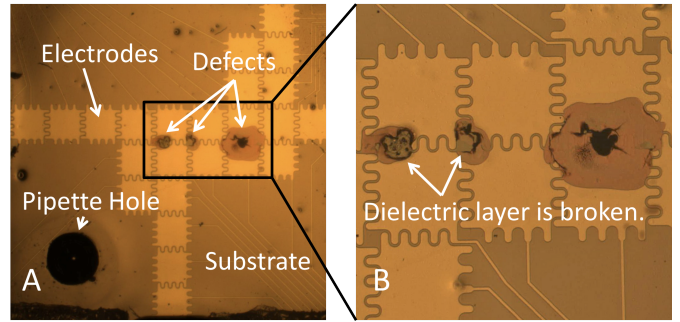


Fig. 1: (a) Image of a fabricated chip with breakdown defects. (b) Zooming into defects. The dielectric layer is broken at these spots so that droplet(s) will directly contact with embedded metal electrodes, leading to the failure of electrowetting and stop the transportation of droplet(s).

Additional causes of defects and incorrect operation include:

- *Geometrical parameter deviation*: The deviation in insulator thickness, electrode length and height between parallel plates may exceed their tolerance value.
- *Change in viscosity of droplets and filler medium*: These can occur during operation due to an unexpected biochemical reaction, or changes in operational environment, e.g., temperature variation.

A consequence of all the above defects is that they impeded droplet transportation during a bioassay and lead to incorrect outcomes. In many cases, the sensing site does not receive any product droplet(s). Fig. 1 shows an example of a biochip fabricated at our laboratory that was tested and found to have a dielectric breakdown defect. The defect site and a closer view of it are highlighted in Fig. 1(b).

### B. Capacitance Sensing

In our work, we have used a capacitance sensing circuit for fault detection at an electrode. The ring oscillator shown in Fig. 2(a) was coupled with a custom digital circuit, implemented in an FPGA, to enable the detection of the presence and absence of nanoliter scale droplets on an electrowetting on dielectric (EWD) platform, which transports droplets by creating an imbalance of interfacial tension between a liquid and an electrode coated with a dielectric layer [3]. Similar feedback strategies were implemented for controlled-volume generation of droplets [11], [12], in particular to demonstrate the use of feedback provided by a ring oscillator circuit to maximize dispensed droplet-volume reproducibility. However, the measurement of droplet volume through such sensing circuits requires a considerable amount of manual intervention, so it is not suitable for cyberphysical integration. Rather than monitoring the volume of droplets, our goal is to test for droplet presence, but this test must be carried out in an autonomous manner. To achieve this goal, we relied on the inverse relationship between droplet volume,  $V$ , and ring oscillator frequency,  $f$ , ( $V \propto C \propto \frac{1}{f}$ ) as well as the ability of a high-speed frequency measurement and comparator to classify signals corresponding to the presence or absence of a droplet. Given an EWD actuation sequence, classification of the presence or absence of a droplet over an EWD electrode allows for real-time detection of potential droplet routing errors that

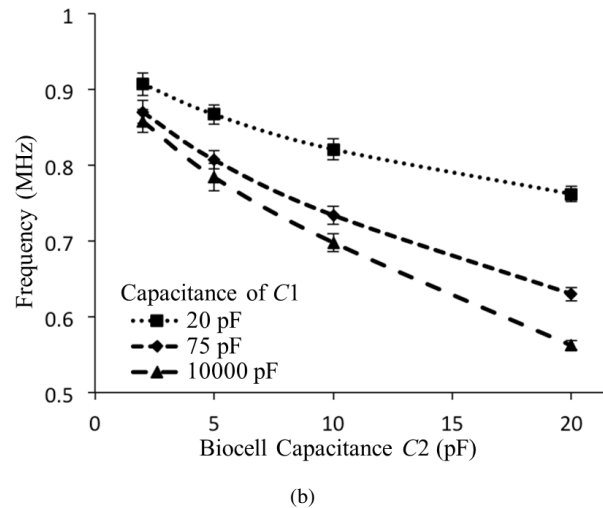
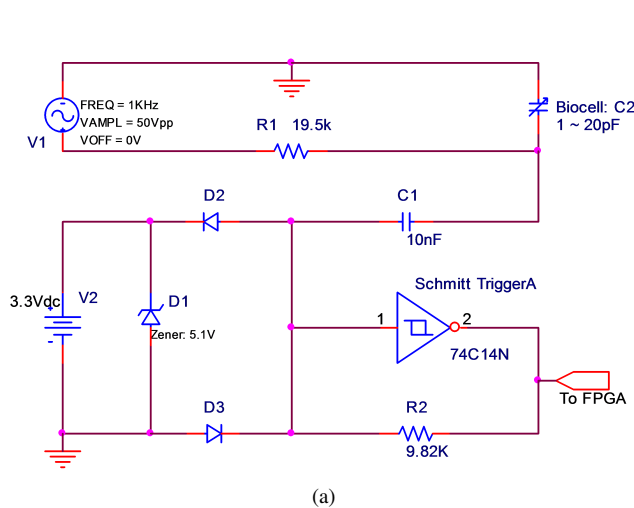


Fig. 2: (a) Ring oscillator circuit used for droplet detection. (b) Frequency response curves of the ring oscillator for three values of  $C_1$ . Note that the sensitivity and linearity of the ring oscillator frequency response increases with increasing values of  $C_1$ .

may occur during a pre-programmed assay. In Fig. 2(b), the capacitance  $C_2$  refers to the capacitance of the “biocell”, i.e., the electrode with the droplet that is being sensed.

The ring oscillator circuit is used to monitor the capacitance between the control and ground electrodes in an EWD actuator. Its output is a 0-3.3 V frequency-encoded square wave, ranging from 750 kHz to 1.5 MHz, with a 50% duty cycle. When a droplet of ionic liquid is present between these electrodes, the majority of the applied electric field forms over the dielectric of the EWD actuator. This decreases the distance of charge separation in the device and results in an increased capacitance for the overall structure, including the droplet. Without a droplet present, the electric field applied for actuation is established over the actuator dielectric as well as the filler medium, i.e., oil or air. This increases the distance over which charge is separated in the device, thereby decreasing the capacitance measured for the overall structure, filler medium inclusive. Thus, when a conductive droplet is present on an EWD actuator/sensor, the measured capacitance will be approximately that of the electrowetting dielectric. And, conversely, when only filler media is present, the measured capacitance is approximately the series capacitance of the actuator dielectric and filler media, an intrinsically lower value than the capacitance of the electrowetting dielectric alone. In Fig. 2(a), the capacitance  $C_1$  is used to increase the difference between the frequency measured for the circuit with a droplet and the circuit without a droplet. A larger  $C_1$  for a fixed  $C_2$  is desired, or vice versa, a smaller  $C_2$  (e.g., by using a thinner dielectric or a material with lower dielectric constant) can be used to increase resolution. Fig. 2(b) shows the relationship between the capacitance  $C_2$  and the oscillation frequency for various values of  $C_1$ .

Electrodes that are equipped with the sensing circuit are designated as checkpoints. For effective error recovery, a number of such checkpoints must be incorporated. Though the above capacitance sensing can be used to detect errors, it is impossible to uniquely locate the site of the defect. From

the set of erroneous readings from the checkpoints, we can generate a set of likely defect sites, and this information can be used to guide the re-routing of droplets for error recovery.

### C. Cyberphysical Error Recovery

When a “missing droplet” error is detected at a checkpoint, we can infer that the defect lies on the path between this checkpoint and the previous checkpoint on the designated droplet route.

As discussed in Section I, sensor feedback can be used to reprogram the digital microfluidic system by generating a new set of electrode actuation sequences. A drawback of prior work [7], [8] is that the recovery is carried out completely in software and all fluidic operations on the chip must be stopped while new actuation sequences are generated. Another drawback of [7], [8] is that a set of electrodes on the biochips must be set aside, or “reserved”, for use during error recovery. Here we adopt a hardware-assisted solution, whereby the assay can proceed without interruptions during recovery, and only droplet routes that involve the checkpoint with errors are stalled. In this way, we are able to carry out bioassays with minimal impact on assay completion time. The error detection and recovery steps are carried out with no user involvement. In fact, the user is oblivious of the occurrence of errors.

The proposed approach therefore shortens the wait time of error recovery. Instead of naïve repetition of fluidic steps, we dynamically re-compute electrode actuation sequences for the biochemical experiments. Multiple errors can be tolerated and multiple droplets can be simultaneously controlled/re-routed on the chip.

## III. IMPLEMENTATION OF ERROR RECOVERY

In this section, we describe algorithmic innovations and the design of the hardware/software interface for real-time error recovery.

### A. Assignment of Checkpoints and Region Division

For capacitance sensing at a checkpoint, the direct connection between driven power source and biochip electrodes is modified and an extra capacitance measurement circuit is added, which consumes a portion of power provided by the power supply. A consequence of sensor insertion at the checkpoints is that droplets move more slowly to the biocell with sensor. The reduction in droplet velocity can be tolerated if the number of checkpoints is not excessive. It is also important to reduce the number of checkpoints in order to minimize the cost of the sensing hardware. The minimum number of checkpoints and their locations depend on the design of the biochip and the intended assays.

Since we do not need to monitor droplets at every clock cycle (rather, we need to periodically test for droplet presence/absence status), we divide a biochip into several regions. A *region* is a combination of several adjacent electrodes, in which multiple microfluidic operations are executed. Each region is associated with a checkpoint. After all the fluidic steps are completed within a region  $R$ , droplets are moved to the checkpoint for testing. Sensor feedback from the checkpoints informs the control software about the possibility of an error within that region. If there is no error, droplets from  $R$  are transported to the next region according to the routing plan encoded in the form of electrode actuation sequences. Otherwise, the error recovery steps are triggered for  $R$ .

With a limited number of checkpoints (one per region), it is difficult to precisely locate a defect site (one or more defective electrodes) within a region. The only information available to us is that a droplet is stuck within a region, and between two checkpoints — the first checkpoint indicated a pass and the second checkpoint indicated a fail. In order to recover from the error, the control software initiates a “rollback” step, whereby a droplet under test retraces its path from the current checkpoint to the previous checkpoint. The rollback is deemed to have been successful when the previous checkpoint once again reports the presence of a droplet (after a known number of clock cycles). Dynamic reconfiguration is triggered by the hardware/software interface, an alternate path computed in software, and new actuation sequences applied to the chip. This approach obviates the need to repeat multiple steps of the assay, especially the steps corresponding to the predecessors of the operations that did not complete correctly.

Based on the fault models listed in Section II-A and on our laboratory experience, such a retracing step is possible in most cases. If retracing fails, i.e., the previous checkpoint does not report a droplet, we conclude the droplet is irreversibly stuck. A new droplet has to be dispensed from the reservoir and the electrodes on the chip between the two checkpoints have to be permanently discarded.

### B. Biochip Layout for Demonstration

We next describe the biochip layout and experiment design for the demonstration of error recovery.

Our experimental digital microfluidic biochip, whose layout is shown in Fig. 3, consists 32 independent electrodes that are each controlled by an independent input pin, is divided into

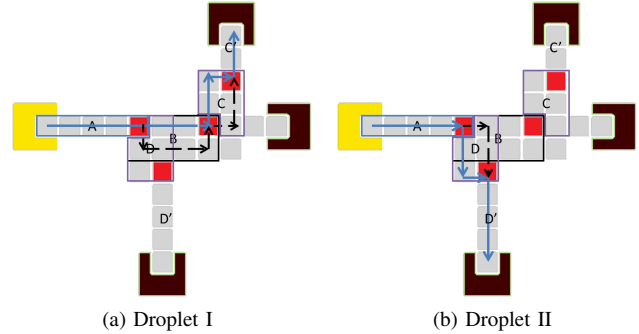


Fig. 3: Biochip layout for our cyberphysical error recovery demo.

four regions. To realize and demonstrate simultaneous control of multiple droplets, two droplets are dispensed from a reservoir (cell marked in yellow) and simultaneously controlled. The first one is transported along Region  $A \Rightarrow B \Rightarrow C \Rightarrow C'$ , while the other droplet's route is Region  $A \Rightarrow D \Rightarrow D'$ . There is an initial route for each region that directly connects inlet and outlet of this region to ensure a shortest path from reservoir to target sink.

The positions of checkpoints are determined to ensure that each region has exactly one checkpoint (cells in red). From our pre-computed actuation sequences, we know the clock cycle when droplets are expected to arrive at checkpoints. The control software (implemented in Matlab) analyzes sensor readouts and determines whether droplets have arrived as expected. If droplets reach checkpoints as planned, the experiment will be continued and droplets will enter the next region. If not, the reconfiguration steps will be triggered automatically, a backup route will be generated in real-time and the new electrode actuation sequences will be immediately fed to the biochip.

Recall that a checkpoint is realized in this work through capacitance sensing. For our experiments, we created defective chips with electrode-open faults by deliberately forcing selected electrode to a low voltage for the duration of experiments. When the experiment begins, two droplets are controlled by software and they follow their respective shortest initial routes (labeled by solid line, in Fig. 3). The capacitance sensing signal is generated when droplets reach the checkpoints and the oscillation frequencies are compared with preset thresholds. Due to variations on the chip surface, the threshold depends on the electrode hence careful calibration is needed before the start of experiments. Based on the outcome of the comparison, the software makes a real-time decision whether it is necessary to activate the back-up path, i.e., send droplets back to previous checkpoints first and take alternative path to bypass the fault (labeled in dashed line, in Fig. 3). All operations are fully automated with no human intervention. Such a setup and its successful implementation is a significant step forward for laboratory biochemical assays.

### C. Interface and Control System

The control system consists of three parts: a desktop, inexpensive computer for generating new electrode actuation sequences, a low-end microcontroller (Arduino for this work),

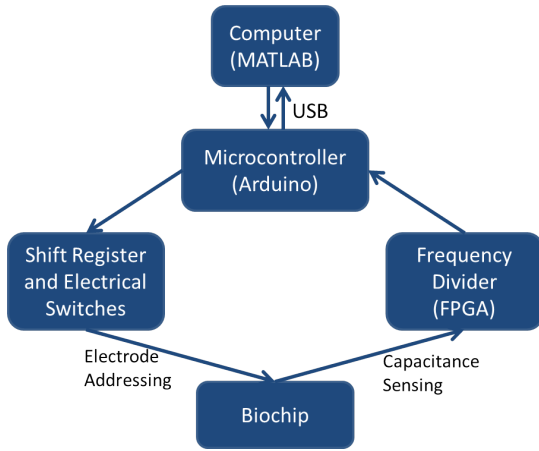


Fig. 4: Schematic of control system setup.

and an FPGA. For synchronous actuation of the 32 electrodes of biochip, a shift register with an output latch is used to control 32 electrical switches. Arduino, as an intermediate microcontroller (Fig. 4), provides the following functionalities: (i) communication with the computer via USB link; (ii) control signals for the shift register; (iii) frequency meter, processing the frequency information readout from the FPGA.

Once a 32-bit vector is sent to Arduino from the computer, a selected output pin of Arduino is pulsed multiple times, thereby communicating these four data bytes to the register in a bit-by-bit fashion. Once all four bytes are transferred to the register, a “parallel output” pin is pulsed to simultaneously transfer all 32 signals.

We need to accurately measure the frequency signal derived from the capacitance sensing circuit (in the range of 750 kHz ~1.5 MHz). The low-cost Arduino microcontroller has a clock of only 7 MHz, hence it is insufficient to measure the oscillation frequency. Therefore, we implemented a frequency division program on an off-the-shelf FPGA, whose clock frequency is more than seven times larger than that of Arduino. Frequency division on the FPGA can real-time reduce the input frequency by 32X and send the modulated square wave to Arduino. Each aggregated capacitance sensing feedback value includes 100 frequency measurements of the modulated signal by Arduino, whose average is compared with a preset threshold to makes a real-time decision on whether to continue the experiment or to use a backup droplet route for error recovery.

An important design challenge arises from the fact that a 1 kHz AC power source is directly connected to the biocell for actuation and inducing droplet motion via electrowetting. The AC power source in close proximity to the capacitance sensor leads to serious interference for the capacitance sensing output, which is a frequency-encoded square wave. To reduce this interference, a 1 ms window is set in the FPGA to accumulate all signals in one period of the AC source before updating the output.

#### IV. EXPERIMENTAL RESULTS AND DEMONSTRATION

In this section, we present experimental results and a demonstration of error recovery through a video.

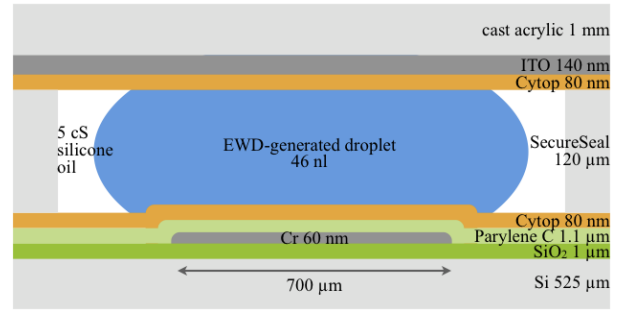


Fig. 5: Cross-section of the fabricated microfluidic biochip.

#### A. Biochip Fabrication and Chip Specifications

As illustrated in Fig. 5, the microfluidic device for our experiments consists of an acrylic top plate and a Si bottom plate. To fabricate the bottom plate, first 1 μm thermal oxide and then 60 nm EBPVD Cr were deposited on a 525 μm thick Si wafer. Second, the Cr layer was lithographically patterned with 32 EWD electrodes and their corresponding chip-to-world contact pads. After this step, 1.1 μm CVD Parylene C dielectric and 80 nm spin-coated Cytop hydrophobic layer were applied.

To fabricate the top plate, pipette ports were CNC-milled on a 1 mm acrylic plate. Subsequently, the acrylic plate was sputtered with a 140 nm ITO grounding electrode. Next, a laser-patterned SecureSeal double-sided adhesive was attached. It serves as a 120 μm thick gasket that provides an optimal confinement of reagents in their respective reservoirs. Afterwards, the fabrication of the top plate was completed with the spin coating of 80 nm Cytop.

Finally, the microfluidic device was assembled by bonding the two plates together via the adhesive SecureSeal gasket. The alignment between the two plates was facilitated by a custom-made alignment guide. The devices were be ready for testing after an overnight vacuum desiccation to evaporate the Cytop solvent. Overall, the device is 31 mm x 24 mm x 1.6 mm in size.

The resulting unit droplet volume, as defined by the 700 μm diameter of electrodes and the 120 μm thick gasket, is approximately 46 nl. Furthermore, each of the four reservoirs has a capacity of 4.5 μl. Herein, at least one reservoir is loaded with 0.08% w/v Tween 20 in DI water, and the remaining volume is filled with 5 cSt silicone oil in order to mitigate droplet evaporation and reduce the droplet actuation voltage.

#### B. Capacitance Estimation and Circuit Optimization

As mentioned above, the EWD platform presented herein made use of EWD actuation electrodes that measured approximately  $700 \times 700 \mu\text{m}^2$  in area,  $A$ , a parylene-C dielectric of 1.1 μm thickness,  $t_d$ , with a dielectric constant of  $\sim 3\epsilon_0$ , an SU-8 defined fluidic channel 160 μm thickness,  $t_0$ , and 2 cSt silicone oil filler medium that also has a dielectric constant of  $\sim 3\epsilon_0$ . Using these parameters, capacitance estimates for the cases when a droplet is present and absent were computed using a simple parallel plate model. Hence, when a droplet is present on an EWD actuator, we expect a capacitance of  $C_p = \frac{3\epsilon_0 A}{t_d} \sim 10\text{pF}$ . Similarly, when a droplet is not present, we

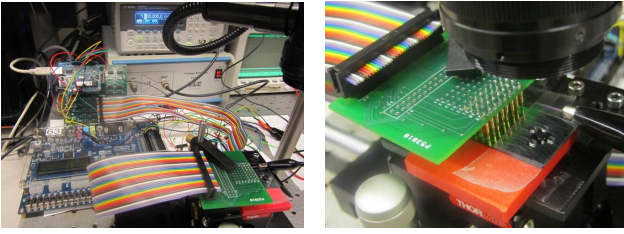


Fig. 6: Demo setup in the laboratory.

expect a capacitance of  $C_a = \left(\frac{t_d+t_0}{3\epsilon_0 A}\right)^{-1} \sim 0.08pF$ . Thus, for the proposed structure, we anticipate an approximate change in capacitance of  $\Delta C = C_p - C_a \sim 10pF$ . These estimates were then used to optimize electrical components in the ring oscillator. Preliminary circuit studies revealed that the coupling capacitor,  $C1$  in Fig. 2(a), greatly affected the sensitivity and linearity of the ring oscillator circuit. Fig. 2(b) shows a family of frequency responses of the ring oscillator circuit for a range of test droplet capacitances,  $C2$ . The plot shows an increase in the magnitude of the frequency response slope, or sensitivity, for increasing values of  $C1$ . In addition, the linearity of the frequency response was found to increase by increasing  $C1$ . In our demo,  $C1$  is  $10pF$ .

### C. Results and Videos

The demo setup is shown in Fig. 6. Several experimental runs were carried out using the fabricated chip, sensing hardware, the hardware/software interface, and the control software described in this paper. A CCD camera was used to capture the video and images were extracted from the recorded video. Videos of error-recovery experiments are available online [13]. A supplementary demonstration video of capacitance sensing is also attached. Droplets were routed as discussed in Section III. Black crosses indicate where the open faults are. The fault-free video shows the initial droplet route. If an error occurs, droplets cannot reach checkpoints as planned and therefore backup routes (lines in red) are enabled to bypass faults. Successful re-routing of droplets was observed in all cases, and snapshots of the experiment are shown in Fig. 7.

### V. CONCLUSION

We have demonstrated fault detection, cyberphysical integration, and dynamic error recovery for a fabricated digital microfluidic biochip. Due to the interactions between multiple energy domains—electrical, fluidic, and mechanical—these devices are especially prone to defects and erroneous droplet operations. Hence the approach described in this paper is a significant step forward for fault tolerance in biochemistry-on-chip. Errors in droplet transportation are detected using capacitance sensors, the test outcome is interpreted by rapid hardware, and software-based recovery is accomplished using dynamic reconfiguration—all without any intervention by a laboratory technician. The hardware/software interface has been realized through seamless interaction between control software, an off-the-shelf microcontroller and a frequency divider implemented on an FPGA. We have reported experimental results for a fabricated silicon device and links [13] to videos have been provided for the experimental demonstration.

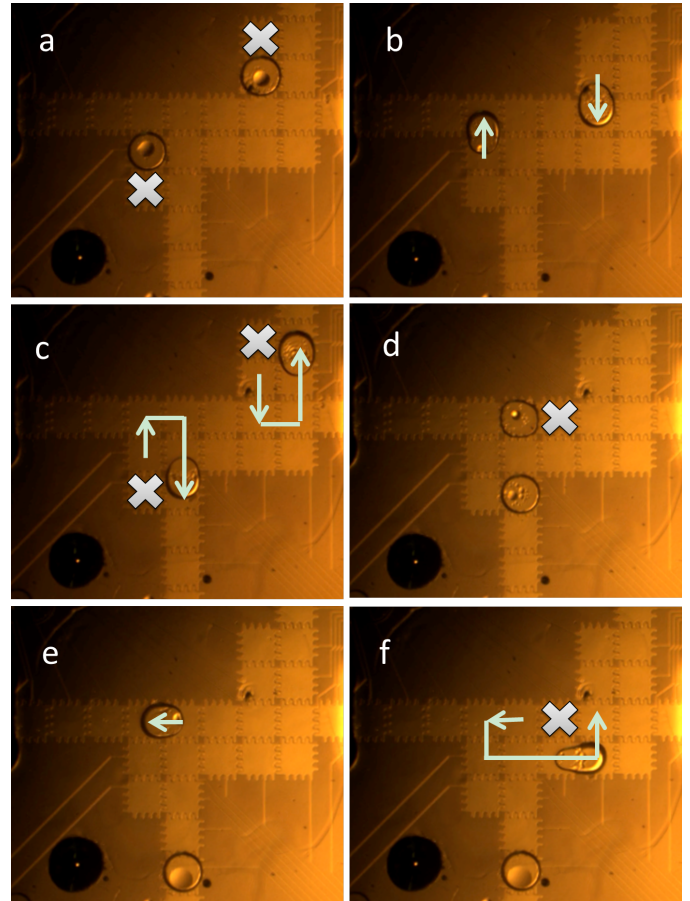


Fig. 7: Frames grabbed from video. Crosses indicate the positions of open faults. (a), (d): Due to defects, droplets are stuck. Checkpoints inform control software about the absence of droplets. (b), (e): Droplets are moved back to the previous checkpoints first. (c), (f): Backup routes are computed to bypass the faults. If droplets reach checkpoints, they will be transported to next regions.

### REFERENCES

- [1] K. Chakrabarty and F. Su, "Digital Microfluidic Biochips: Synthesis, Testing, and Reconfiguration Techniques", CRC Press, FL, 2006
- [2] R. B. Fair et al., "Chemical and biological applications of digital-microfluidic devices", IEEE Design & Test of Computers, vol. 24, 2007.
- [3] M.G. Pollack et al., "Electrowetting-based actuation of liquid droplets for microfluidic applications", Applied Physics Letters, vol. 77, 2000.
- [4] M. Iyengar and M. McGuire, "Imprecise and qualitative probability in systems biology", International Conference on Systems Biology, 2007.
- [5] O. Levenspiel, "Chemical Reaction Engineering", Wiley, NY, 1999.
- [6] C. A. Mein et al., "Evaluation of single nucleotide polymorphism typing with invader on PCR amplicons and its automation", Genome Res., vol. 10, pp. 330-343, 2000.
- [7] Y. Luo, K. Chakrabarty and T.-Y. Ho, "A cyberphysical synthesis approach for error recovery in digital microfluidic biochips", IEEE/ACM Design, Automation and Test in Europe (DATE) Conference, 2012.
- [8] X. Zhang, F. Proosdij, and H. G. Kerkhoff, "A droplet routing technique for fault-tolerant digital microfluidic devices", in Proc. IEEE Int. Mixed-Signal Sensors Syst. Test Workshop, Jun. 2008, pp. 1–7.
- [9] T. Xu and K. Chakrabarty, "Fault modeling and functional test methods for digital microfluidic biochips", IEEE Transactions for Biomedical Circuits and Systems, vol. 3, pp. 241-253, August 2009.
- [10] J. H. Song et al., "A scaling model for electrowetting-on-dielectric microfluidic actuators", Microfluidics and Nanofluidics, pp. 75–89, 2009.
- [11] H. Ren, R. B. Fair, and M. G. Pollack, "Automated on-chip droplet dispensing with volume control by electro-wetting actuation and capacitance metering," Sensors and Actuators B, vol. 98, pp. 319-327, 1004.
- [12] J. Gong and C. J. Kim, "All-electronic droplet generation on-chip with real-time feedback control for EWOD digital microfluidics", Lab on a Chip, vol. 8, pp. 898-906, 2008.
- [13] [http://microfluidics.ee.duke.edu/Published\\_Videos/2013\\_DATE/](http://microfluidics.ee.duke.edu/Published_Videos/2013_DATE/)